DYNAMIC MODELLING, ESTIMATION, AND CONTROL FOR PRECISION POINTING OF AN ATMOSPHERIC BALLOON PLATFORM

David Evan Zlotnik[1] and James Richard Forbes[2]
[1]*Department of Mechanical Engineering, McGill University, Montreal, QC, Canada*
[2]*Department of Aerospace Engineering, University of Michigan, Ann Arbor, MI, USA*
E-mail: david.zlotnik@mail.mcgill.ca; forbesrj@umich.edu

Received July 2013, Accepted March 2014
No. 13-CSME-193, E.I.C. Accession 3651

ABSTRACT
In this paper we consider the dynamic modelling, estimation and control of an atmospheric balloon platform. The platform is modelled as a rigid body constrained to move with a three dimensional pendulum. We investigate the dynamics of the system and derive the equations of motion from first principles. A nonlinear estimator that evolves on the special orthogonal group of rigid-body rotations, denoted $SO(3)$, is implemented and used in conjunction with a proportional derivative (PD) compensator to control the yaw angle of the platform. A simulation is conducted, and the results demonstrate successful estimation and yaw control.

Keywords: balloon platform modelling; rotation-matrix estimation; attitude control.

LA MODÉLISATION DYNAMIQUE, L'ESTIMATION ET LE CONTRÔLE POUR LE GUIDAGE DE PRÉCISION D'UNE PLATEFORME DE BALLON ATMOSPHÉRIQUE

RÉSUMÉ
Dans cet article, on considère la modélisation dynamique, l'estimation et le contrôle d'une plateforme de ballon atmosphérique. La plateforme est modélisée comme un corps rigide contraint de se déplacer avec une pendule à trois dimensions. On examine la dynamique du système et dérive les équations du mouvement à partir des principes fondamentaux. Un estimateur non linéaire qui évolue sur un groupe orthogonal spécial, noté SO(3), est mis en œuvre et utilisé en conjonction avec un compensateur proportionnel dérivé (PD) pour contrôler l'angle de lacet de la plateforme. Une simulation est effectuée et les résultats démontrent la réussite de l'estimation et du contrôle de l'angle de lacet.

Mots-clés : modélisation plateforme de ballon; estimation de la matrice de rotation; contrôle d'attitude.

1. INTRODUCTION

Physicists are concerned with certain properties of the universe, such as the rate at which the universe is expanding. In order to determine the rate at which the universe is expanding, physicists must precisely measure the size of astronomical objects, such as supernova. To do so, ground-based telescopes are used. The accuracy of these telescopes can be greatly improved if properly calibrated using a microwave light source at a known distance and elevation.

The McGill University High Altitude Balloon (McHAB) team has designed, developed and launched a low-cost atmospheric balloon-borne platform, or gondola, that will be used to carry such a microwave light source. However, the platform currently lacks an adequate attitude control system that will enable precision pointing of the microwave light source to be pointed in the direction of ground-based telescopes. In this paper the dynamic modelling, estimation and control of such a balloon platform is considered in detail.

Attitude control, that is the control of the orientation and angular velocity of a body, is a nonlinear control problem. The attitude control system must overcome external disturbances, allowing the body to be stabilized and pointed in a desired direction. This requires the use of sensors to estimate the attitude, and actuators to control it [1]. The attitude of a body is completely described by a rotation matrix [2]. However, typically attitude estimation is accomplished by first parameterizing the rotation matrix using a quaternion, and then using an extended Kalman filter to estimate the quaternion [3]. For example, in [4–6] the attitude of a balloon platform is estimated using various sensors and an extended Kalman filter. Despite its popularity, the Kalman filter has been found to perform poorly when adapted to nonlinear systems, especially when coupled with low-cost measurement units [7, 8]. Recently, nonlinear observers that estimate the rotation matrix directly without any sort of rotation-matrix parameterization have been developed [7–10]. The novel contribution of this work is building on [7, 9] by adapting the proposed attitude estimator to the balloon platform being constructed by the McHAB team and observing the performance of the estimator in conjunction with yaw axis feedback control.

The remainder of this paper is as follows. We review notation and give a description of the hardware used on the platform in Section 2. In Section 3, the kinematics and dynamics of the proposed platform model are considered, and the equations of motion are derived. Section 4 is where we review the estimator proposed in [7, 9] and adapt it for use with the balloon platform. We simulate the platform dynamics and present the results in Section 6 and close with concluding remarks in Section 7.

2. PRELIMINARIES

2.1. Notation

A physical vector, $\underrightarrow{u}$, can be written as

$$\underrightarrow{u} = \underrightarrow{\mathscr{F}}_a^{\mathsf{T}} \mathbf{u}_a,$$

where $\underrightarrow{\mathscr{F}}_a = [\underrightarrow{a}_1 \;\; \underrightarrow{a}_2 \;\; \underrightarrow{a}_3]^{\mathsf{T}}$ is the vectrix associated with reference frame "a", denoted $\mathscr{F}_a$, and $\mathbf{u}_a = [u_{a1} \;\; u_{a2} \;\; u_{a3}]^{\mathsf{T}} \in \mathbb{R}^3$ are the components of $\underrightarrow{u}$ expressed in $\mathscr{F}_a$. The cross product of two physical vectors can be written as [2]

$$\underrightarrow{u} \times \underrightarrow{v} = \mathbf{u}_a^{\mathsf{T}} \underrightarrow{\mathscr{F}}_a \times \underrightarrow{\mathscr{F}}_a^{\mathsf{T}} \mathbf{v}_a = \underrightarrow{\mathscr{F}}_a^{\mathsf{T}} \mathbf{u}_a^{\times} \mathbf{v}_a,$$

where $(\cdot)^{\times} : \mathbb{R}^3 \to \mathfrak{so}(3)$ with [11]

$$\mathfrak{so}(3) = \{\mathbf{S} \in \mathbb{R}^{3\times 3} \mid \mathbf{S}^T = -\mathbf{S}\},$$

such that

$$\mathbf{u}_a^{\times} = \begin{bmatrix} 0 & -u_{a3} & u_{a2} \\ u_{a3} & 0 & -u_{a1} \\ -u_{a2} & u_{a1} & 0 \end{bmatrix}.$$

Given $\underrightarrow{\mathscr{F}}_b^{\mathsf{T}}\mathbf{v}_b = \underrightarrow{\mathscr{F}}_i^{\mathsf{T}}\mathbf{v}_i$ the relationship between $\mathbf{v}_b$ and $\mathbf{v}_i$ can be found by taking the dot product with $\underrightarrow{\mathscr{F}}_b$ to obtain [2]

$$\begin{aligned} \underbrace{\underrightarrow{\mathscr{F}}_b \cdot \underrightarrow{\mathscr{F}}_b^{\mathsf{T}}}_{\mathbf{1}}\mathbf{v}_b &= \underrightarrow{\mathscr{F}}_b \cdot \underrightarrow{\mathscr{F}}_i^{\mathsf{T}}\mathbf{v}_i \\ \mathbf{v}_b &= \mathbf{C}_{bi}\mathbf{v}_i, \end{aligned}$$

where $\mathbf{C}_{bi} = \underrightarrow{\mathscr{F}}_b \cdot \underrightarrow{\mathscr{F}}_i^{\mathsf{T}} \in SO(3)$ is the rotation matrix that transforms the components of a physical vector resolved in $\mathscr{F}_i$ to $\mathscr{F}_b$ and $SO(3)$ denotes the special orthogonal group of rigid-body rotations defined as

$$SO(3) = \{\mathbf{C} \in \mathbb{R}^{3\times 3} \mid \mathbf{C}^{\mathsf{T}}\mathbf{C} = \mathbf{1},\ \det(\mathbf{C}) = +1\},$$

where $\mathbf{1}$ is the identity matrix [11].

2.2. McHAB System Overview

The atmospheric balloon system built by the McHAB team is shown in Fig. 1(a). The system consists of a balloon, tether, parachute (to reduce the decent rate), and a platform. The balloon platform is equipped with an inertial measurement unit (IMU) and a Raspberry Pi single-board computer. The IMU is a DIYDrones ArduIMU+ V3, which contains a 3-axis accelerometer, 3-axis gyroscope and a 3-axis magnetometer. Assuming a constant ascent rate, the accelerometer can be used along with the magnetometer and gyroscope for attitude determination. The actuator used for control is a brushless DC motor with a high moment of inertia. This was done to avoid manually machining a flywheel. In this paper, the motor dynamics have been neglected since they operate at a much higher bandwidth. The motor is aligned with the yaw axis of the platform and produces torque about this axis. The McHAB platform requires secondary control systems to control the pitch angle of the microwave source as well as to dampen rolling motion, however these systems are not considered in this paper. For additional details of the McHAB system, see [12].

3. PLATFORM MODEL

Consider the balloon platform model shown in Fig. 1(b). The platform itself is modelled as a rigid body and is denoted $\mathscr{R}$. To model the swinging motion of the platform during flight, we will consider $\mathscr{R}$ to be constrained to move at the end of a pendulum, denoted body $\mathscr{P}$. We model the pendulum as a rigid body. This is reasonable since, in the experience of the McHAB team, the tether will remain in tension during ascent. Though $\mathscr{R}$ is constrained to move with the pendulum, it is free to rotate in three dimensions. We attach a reference frame, $\mathscr{F}_b$, with associated vectrix $\underrightarrow{\mathscr{F}}_b = [\underrightarrow{b}_1 \quad \underrightarrow{b}_2 \quad \underrightarrow{b}_3]^{\mathsf{T}}$, to $\mathscr{R}$ at its centre of mass. Another reference frame, $\mathscr{F}_p$, with associated vectrix $\underrightarrow{\mathscr{F}}_p = [\underrightarrow{p}_1 \quad \underrightarrow{p}_2 \quad \underrightarrow{p}_3]^{\mathsf{T}}$, is attached to $\mathscr{P}$ with its origin located at the centre of the inertial frame, $\mathscr{F}_i$. The pendulum $\mathscr{P}$, has one end fixed to the centre of $\mathscr{F}_i$ and another attached to $\mathscr{R}$ at point o.

3.1. Kinematic Relations and Constraints

In order to describe the motion of the rigid body and pendulum, we require their respective angular velocities. Let $\underrightarrow{\omega}^{bi} = \underrightarrow{\mathscr{F}}_b^{\mathsf{T}}\boldsymbol{\omega}_b^{bi}$ and $\underrightarrow{\omega}^{pi} = \underrightarrow{\mathscr{F}}_p^{\mathsf{T}}\boldsymbol{\omega}_p^{pi}$ be the angular velocities of $\mathscr{F}_b$ and $\mathscr{F}_p$ relative to $\mathscr{F}_i$, respectively. The orientation of frames $\mathscr{F}_b$ and $\mathscr{F}_p$ relative to $\mathscr{F}_i$ can be described by the rotation ma-

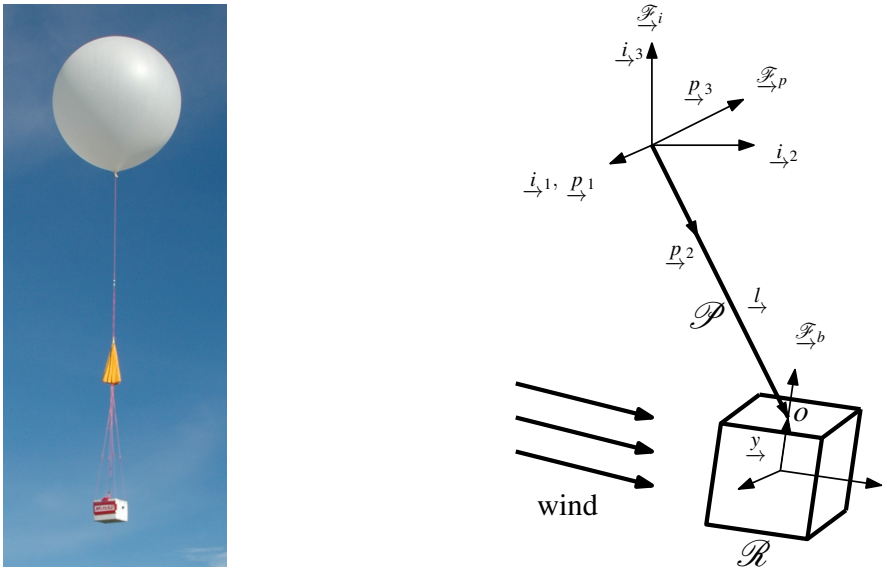

(a) (b)

Fig. 1. (a) Actual balloon platform and (b) platform model.

trices $\mathbf{C}_{bi}$ and $\mathbf{C}_{pi}$, respectively. These rotation matrices can be defined using any Euler angle sequence, $\boldsymbol{\theta}^{bi} = [\alpha_b \;\; \beta_b \;\; \gamma_b]^{\mathsf{T}}$ or $\boldsymbol{\theta}^{pi} = [\alpha_p \;\; \beta_p \;\; \gamma_p]^{\mathsf{T}}$. We will require the relationship between angular velocity and the time rate of change of the Euler angles [13],

$$\boldsymbol{\omega}_a^{ai} = \mathbf{S}_a^{ai} \dot{\boldsymbol{\theta}}^{ai}, \tag{1}$$

where $\mathbf{S}_a^{ai} = \mathbf{S}_a^{ai}(\alpha_a, \beta_a) \in \mathbb{R}^{3\times 3}$ is the appropriate mapping matrix between the Euler angle rates and the angular velocities, and a replaces b or p. The kinematics of $\mathscr{R}$ and $\mathscr{P}$ are described by [2],

$$\dot{\mathbf{C}}_{bi} + \boldsymbol{\omega}_b^{bi\times} \mathbf{C}_{bi} = \mathbf{0}, \tag{2}$$

and

$$\dot{\mathbf{C}}_{pi} + \boldsymbol{\omega}_p^{pi\times} \mathbf{C}_{pi} = \mathbf{0},$$

respectively.

Constraint Equations

Since we have constrained $\mathscr{R}$ to move with $\mathscr{P}$, the position of $\mathscr{F}_b$ can be described by

$$\underrightarrow{r}^{\,bi} = \underrightarrow{l} - \underrightarrow{y},$$

where $\underrightarrow{r}^{\,bi}$ is the position of the origin of $\mathscr{F}_b$ relative to the origin of $\mathscr{F}_i$, $\underrightarrow{l}$ is the position of point o relative to the origin of $\mathscr{F}_p$, and $\underrightarrow{y}$ is the position of point o relative to the origin of $\mathscr{F}_b$. Then,

$$\begin{aligned} \underrightarrow{r}^{\,bi^{\bullet}} &= (\underrightarrow{l}^{\,\circ} + \underrightarrow{\omega}^{\,pi} \times \underrightarrow{l}) - (\underrightarrow{y}' + \underrightarrow{\omega}^{\,bi} \times \underrightarrow{y}), \\ \dot{\mathbf{r}}_i^{bi} &= -\mathbf{C}_{pi}^{\mathsf{T}} \boldsymbol{\ell}_p^{\times} \boldsymbol{\omega}_p^{pi} + \mathbf{C}_{bi}^{\mathsf{T}} \mathbf{y}_b^{\times} \boldsymbol{\omega}_b^{bi}, \end{aligned} \tag{3}$$

where $(\cdot)^{\bullet}$, $(\cdot)^{\circ}$ and $(\cdot)'$ indicate time derivatives with respect to $\mathscr{F}_i$, $\mathscr{F}_p$ and $\mathscr{F}_b$ respectively. This constraint equation can be written as

$$\underbrace{\begin{bmatrix} \mathbf{1} & -\mathbf{C}_{bi}^{\mathsf{T}}\mathbf{y}_b^{\times}\mathbf{S}_b^{bi} & \mathbf{C}_{pi}^{\mathsf{T}}\boldsymbol{\ell}_p^{\times}\mathbf{S}_p^{pi} \end{bmatrix}}_{\boldsymbol{\Xi}} \begin{bmatrix} \dot{\mathbf{r}}_b^{bi} \\ \dot{\boldsymbol{\theta}}^{bi} \\ \dot{\boldsymbol{\theta}}^{pi} \end{bmatrix} = \mathbf{0}.$$

Note that in this case $\dot{\mathbf{r}}_b^{bi}$ is dependent on $\dot{\boldsymbol{\theta}}^{bi}$ and $\dot{\boldsymbol{\theta}}^{pi}$. From Eq. (3), we can express $\boldsymbol{\nu} = [\dot{\mathbf{r}}_i^{bi^{\mathsf{T}}} \;\; \boldsymbol{\omega}_b^{bi^{\mathsf{T}}} \;\; \boldsymbol{\omega}_p^{pi^{\mathsf{T}}}]^{\mathsf{T}}$ as

$$\boldsymbol{\nu} = \underbrace{\begin{bmatrix} \mathbf{C}_{bi}^{\mathsf{T}}\mathbf{y}_b^{\times} & -\mathbf{C}_{pi}^{\mathsf{T}}\boldsymbol{\ell}_p^{\times} \\ \mathbf{1} & \mathbf{0} \\ \mathbf{0} & \mathbf{1} \end{bmatrix}}_{\boldsymbol{\Pi}} \underbrace{\begin{bmatrix} \dot{\boldsymbol{\omega}}_b^{bi} \\ \dot{\boldsymbol{\omega}}_p^{pi} \end{bmatrix}}_{\tilde{\boldsymbol{\nu}}}, \tag{4}$$

and recalling Eq. (1) we can write the above in terms of the Euler angles as

$$\begin{bmatrix} \dot{\mathbf{r}}_i^{bi} \\ \dot{\boldsymbol{\theta}}^{bi} \\ \dot{\boldsymbol{\theta}}^{pi} \end{bmatrix} = \underbrace{\begin{bmatrix} \mathbf{C}_{bi}^{\mathsf{T}}\mathbf{y}_b^{\times}\mathbf{S}_b^{bi} & -\mathbf{C}_{pi}^{\mathsf{T}}\boldsymbol{\ell}_p^{\times}\mathbf{S}_p^{pi} \\ \mathbf{1} & \mathbf{0} \\ \mathbf{0} & \mathbf{1} \end{bmatrix}}_{\boldsymbol{\Gamma}} \begin{bmatrix} \dot{\boldsymbol{\theta}}^{bi} \\ \dot{\boldsymbol{\theta}}^{pi} \end{bmatrix}.$$

Note that it can be easily verified that

$$\boldsymbol{\Gamma}^{\mathsf{T}}\boldsymbol{\Xi}^{\mathsf{T}} = \mathbf{0}, \tag{5}$$

a relation that will be of importance later.

3.2. Deriving the Equations of Motion

Both the Lagrangian and the Newton–Euler method can be used to solve for the equations of motion. We will use the Lagrangian approach in this paper because we need the kinetic and potential energy to validate the dynamics of the model in simulation. Lagrange's equation for constrained systems is

$$\frac{d}{dt}\left(\frac{\partial L}{\partial \dot{\mathbf{q}}}\right)^{\mathsf{T}} - \left(\frac{\partial L}{\partial \mathbf{q}}\right)^{\mathsf{T}} = \boldsymbol{\Xi}^{\mathsf{T}}\boldsymbol{\lambda} + \boldsymbol{f}, \tag{6}$$

where $L = T - V$ is the Lagrangian, $\mathbf{q}$ are the generalized coordinates, $\boldsymbol{f}$ are the generalized forces, and $\boldsymbol{\lambda}$ are the Lagrange multipliers associated with the constraint equations. In order to formulate the Lagrangian we need to construct the kinetic energy, T, and the potential energy, V, in terms of the generalized coordinates [13],

$$\mathbf{q} = \begin{bmatrix} \mathbf{r}_i^{bi^{\mathsf{T}}} & \boldsymbol{\theta}^{bi^{\mathsf{T}}} & \boldsymbol{\theta}^{pi^{\mathsf{T}}} \end{bmatrix}^{\mathsf{T}}. \tag{7}$$

Kinetic and Potential Energy

The kinetic and potential energy of $\mathscr{R}$ is

$$T_{\mathscr{R}} = \tfrac{1}{2} m_{\mathscr{R}} \dot{\mathbf{r}}_i^{bi^{\mathsf{T}}} \dot{\mathbf{r}}_i^{bi} + \tfrac{1}{2} \boldsymbol{\omega}_b^{bi^{\mathsf{T}}} \mathbf{I}_b^{\mathscr{R}b} \boldsymbol{\omega}_b^{bi}, \tag{8}$$

and

$$V_{\mathscr{R}} = -m_{\mathscr{R}} g \mathbf{r}_i^{bi^{\mathsf{T}}} \mathbf{1}_3, \tag{9}$$

respectively, where $m_{\mathscr{R}}$ is the mass of $\mathscr{R}$, $\mathbf{I}_b^{\mathscr{R}b}$ is the moment of inertia of $\mathscr{R}$ taken about its centre of mass expressed in $\mathscr{F}_b$, g is the constant acceleration due to gravity and $\mathbf{1}_3 = [0 \;\; 0 \;\; 1]^\mathsf{T}$ [14]. The kinetic and potential energy of $\mathscr{P}$ is,

$$T_{\mathscr{P}} = \tfrac{1}{2}\boldsymbol{\omega}_p^{pi^\mathsf{T}} \mathbf{J}_p^{\mathscr{P}p} \boldsymbol{\omega}_p^{pi}, \tag{10}$$

and

$$V_{\mathscr{P}} = -\tfrac{1}{2} m_{\mathscr{P}} g \boldsymbol{\ell}_p^\mathsf{T} \mathbf{C}_{pi} \mathbf{1}_3, \tag{11}$$

respectively, where $m_{\mathscr{P}}$ is the mass of $\mathscr{P}$ and $\mathbf{J}_p^{\mathscr{P}p}$ is the moment of inertia of $\mathscr{P}$ relative to the origin of $\mathscr{F}_p$ resolved in $\mathscr{F}_p$. Combining Eqs. (8) and (10) we obtain the expression for the total kinetic energy as

$$\begin{aligned} T &= \tfrac{1}{2} m_{\mathscr{R}} \dot{\mathbf{r}}_i^{bi^\mathsf{T}} \dot{\mathbf{r}}_i^{bi} + \tfrac{1}{2} \boldsymbol{\omega}_b^{bi^\mathsf{T}} \mathbf{I}_b^{\mathscr{R}b} \boldsymbol{\omega}_b^{bi} + \tfrac{1}{2} \boldsymbol{\omega}_p^{pi^\mathsf{T}} \mathbf{J}_p^{\mathscr{P}p} \boldsymbol{\omega}_p^{pi} \\ &= \tfrac{1}{2} \begin{bmatrix} \dot{\mathbf{r}}_b^{bi^\mathsf{T}} & \boldsymbol{\omega}_b^{bi^\mathsf{T}} & \boldsymbol{\omega}_p^{pi^\mathsf{T}} \end{bmatrix}^\mathsf{T} \underbrace{\begin{bmatrix} m_{\mathscr{R}}\mathbf{1} & \mathbf{0} & \mathbf{0} \\ \mathbf{0} & \mathbf{I}_b^{\mathscr{R}b} & \mathbf{0} \\ \mathbf{0} & \mathbf{0} & \mathbf{J}_p^{\mathscr{P}p} \end{bmatrix}}_{\mathbf{M}} \begin{bmatrix} \dot{\mathbf{r}}_b^{bi} \\ \boldsymbol{\omega}_b^{bi} \\ \boldsymbol{\omega}_p^{pi} \end{bmatrix} \\ &= \tfrac{1}{2} \boldsymbol{\nu}^\mathsf{T} \mathbf{M} \boldsymbol{\nu}. \end{aligned}$$

Similarly, combining Eqs. (9) and (11) gives the total potential energy

$$V = -m_{\mathscr{R}} g \mathbf{r}_i^{bi^\mathsf{T}} \mathbf{1}_3 - \tfrac{1}{2} m_{\mathscr{P}} g \boldsymbol{\ell}_p^\mathsf{T} \mathbf{C}_{pi} \mathbf{1}_3. \tag{12}$$

It remains to express T in terms of the generalized coordinates. Recalling Eq. (1), T can be rewritten as

$$T = \tfrac{1}{2} \dot{\mathbf{q}}^\mathsf{T} \mathbf{S}^\mathsf{T} \mathbf{M} \mathbf{S} \dot{\mathbf{q}}, \tag{13}$$

where

$$\mathbf{S} = \begin{bmatrix} \mathbf{1} & \mathbf{0} & \mathbf{0} \\ \mathbf{0} & \mathbf{S}_b^{bi} & \mathbf{0} \\ \mathbf{0} & \mathbf{0} & \mathbf{S}_p^{pi} \end{bmatrix}.$$

Now, the Lagrangian can be formed as

$$L = T - V = \tfrac{1}{2} \dot{\mathbf{q}}^\mathsf{T} \mathbf{S}^\mathsf{T} \mathbf{M} \mathbf{S} \dot{\mathbf{q}} + m_{\mathscr{R}} g \mathbf{r}_i^{bi^\mathsf{T}} \mathbf{1}_3 + \tfrac{1}{2} m_{\mathscr{P}} g \boldsymbol{\ell}_p^\mathsf{T} \mathbf{C}_{pi} \mathbf{1}_3.$$

Generalized Torques

The only external torques that will be considered in our model is $\underrightarrow{\tau}^{\,d} = \underrightarrow{\mathscr{F}}_b \boldsymbol{\tau}_b^d$ with $\boldsymbol{\tau}_b^d \in \mathbb{R}^3$, that is the torque induced on the platform by the wind and the disturbance due to balloon rotation acting through the tether on the platform. To find $\boldsymbol{\tau}_b^d$ the method of virtual work will be employed [13]. The virtual work done due to the disturbance torque is

$$\begin{aligned} \delta W &= \underrightarrow{\tau}^{\,d} \cdot \underrightarrow{\mathscr{F}}_b^\mathsf{T} \mathbf{S}_b^{bi} \delta \boldsymbol{\theta}^{bi} \\ &= \delta \mathbf{q}^\mathsf{T} \mathbf{S}^\mathsf{T} \underbrace{\begin{bmatrix} \mathbf{0} \\ \boldsymbol{\tau}_b^d \\ \mathbf{0} \end{bmatrix}}_{\bar{\boldsymbol{\tau}}_b^d} \\ &= \delta \mathbf{q}^\mathsf{T} \mathbf{S}^\mathsf{T} \bar{\boldsymbol{\tau}}_b^d, \end{aligned}$$

where $\mathbf{S}^{\mathsf{T}}\bar{\boldsymbol{\tau}}_b^d$ is the generalized disturbance torque. We will also consider $\underrightarrow{\tau}^c = \underrightarrow{\mathscr{F}}_b \boldsymbol{\tau}_b^c$ with $\boldsymbol{\tau}_b^c \in \mathbb{R}^3$, a control torque produced by actuators onboard the platform. The virtual work done due to the control torque is

$$\begin{aligned}
\delta W &= \underrightarrow{\tau}^c \cdot \underrightarrow{\mathscr{F}}_b^{\mathsf{T}} \mathbf{S}_b^{bi} \delta\boldsymbol{\theta}^{bi} \\
&= \delta\mathbf{q}^{\mathsf{T}} \mathbf{S}^{\mathsf{T}} \begin{bmatrix} \mathbf{0} \\ \boldsymbol{\tau}_b^c \\ \mathbf{0} \end{bmatrix} \\
&= \delta\mathbf{q}^{\mathsf{T}} \mathbf{S}^{\mathsf{T}} \bar{\boldsymbol{\tau}}_b^c,
\end{aligned}$$

where $\mathbf{S}^{\mathsf{T}}\bar{\boldsymbol{\tau}}_b^c$ is the generalized torque due to the onboard actuators.

Equations of Motion

Omitting details for brevity, Eq. (6) gives

$$\mathbf{S}^{\mathsf{T}} (\mathbf{M}\dot{\boldsymbol{\nu}} + \boldsymbol{\Omega}\mathbf{M}\boldsymbol{\nu} + \mathbf{a}) = \boldsymbol{\Xi}^{\mathsf{T}}\boldsymbol{\lambda} + \mathbf{S}^{\mathsf{T}}(\bar{\boldsymbol{\tau}}_b^d + \bar{\boldsymbol{\tau}}_b^c), \tag{14}$$

where

$$\boldsymbol{\Omega} = \begin{bmatrix} \mathbf{0} & \mathbf{0} & \mathbf{0} \\ \mathbf{0} & \boldsymbol{\omega}_b^{bi\times} & \mathbf{0} \\ \mathbf{0} & \mathbf{0} & \boldsymbol{\omega}_p^{pi\times} \end{bmatrix}, \quad \text{and} \quad \mathbf{a} = \begin{bmatrix} -m_{\mathscr{R}} g \mathbf{1}_3 \\ \mathbf{0} \\ -\frac{1}{2} m_{\mathscr{P}} g \boldsymbol{\ell}_b^{\times} \mathbf{C}_{pi} \mathbf{1}_3 \end{bmatrix}.$$

3.3. Expressing the Equations of Motion in Terms of the Independent Generalized Coordinates

We have derived the equations of motion in terms of the dependent generalized coordinates, $\boldsymbol{\nu}$. We will now employ the null space method [13], also known as the natural orthogonal compliment method [15, 16], to express the equations of motion in terms of the independent generalized coordinates, $\tilde{\boldsymbol{\nu}}$. This will allow us to avoid calculating the Lagrange multipliers, $\boldsymbol{\lambda}$, as well as reducing the number of states that must be integrated during simulation [13].

Multiplying Eq. (14) by $\boldsymbol{\Gamma}^{\mathsf{T}}$ and recalling from Eq. (5) that $\boldsymbol{\Gamma}^{\mathsf{T}}\boldsymbol{\Xi}^{\mathsf{T}} = \mathbf{0}$ yields

$$\boldsymbol{\Gamma}^{\mathsf{T}}\mathbf{S}^{\mathsf{T}} (\mathbf{M}\dot{\boldsymbol{\nu}} + \boldsymbol{\Omega}\mathbf{M}\boldsymbol{\nu} + \mathbf{a}) = \boldsymbol{\Gamma}^{\mathsf{T}}\mathbf{S}^{\mathsf{T}}(\bar{\boldsymbol{\tau}}_b^d + \bar{\boldsymbol{\tau}}_b^c). \tag{15}$$

Simplifying $\boldsymbol{\Gamma}^{\mathsf{T}}\mathbf{S}^{\mathsf{T}}$, we find that

$$\begin{aligned}
\boldsymbol{\Gamma}^{\mathsf{T}}\mathbf{S}^{\mathsf{T}} &= \begin{bmatrix} (\mathbf{C}_{bi}^{\mathsf{T}}\mathbf{y}_b^{\times}\mathbf{S}_b^{bi})^{\mathsf{T}} & \mathbf{1} & \mathbf{0} \\ (-\mathbf{C}_{pi}^{\mathsf{T}}\boldsymbol{\ell}_p^{\times}\mathbf{S}_p^{pi})^{\mathsf{T}} & \mathbf{0} & \mathbf{1} \end{bmatrix} \begin{bmatrix} \mathbf{1} & \mathbf{0} & \mathbf{0} \\ \mathbf{0} & \mathbf{S}_b^{bi^{\mathsf{T}}} & \mathbf{0} \\ \mathbf{0} & \mathbf{0} & \mathbf{S}_p^{pi^{\mathsf{T}}} \end{bmatrix} \\
&= \begin{bmatrix} (\mathbf{C}_{bi}^{\mathsf{T}}\mathbf{y}_b^{\times}\mathbf{S}_b^{bi})^{\mathsf{T}} & \mathbf{S}_b^{bi^{\mathsf{T}}} & \mathbf{0} \\ (-\mathbf{C}_{pi}^{\mathsf{T}}\boldsymbol{\ell}_p^{\times}\mathbf{S}_p^{pi})^{\mathsf{T}} & \mathbf{0} & \mathbf{S}_p^{pi^{\mathsf{T}}} \end{bmatrix} \\
&= \underbrace{\begin{bmatrix} \mathbf{S}_b^{bi^{\mathsf{T}}} & \mathbf{0} \\ \mathbf{0} & \mathbf{S}_p^{pi^{\mathsf{T}}} \end{bmatrix}}_{\tilde{\mathbf{S}}^{\mathsf{T}}} \underbrace{\begin{bmatrix} -\mathbf{y}_b^{\times}\mathbf{C}_{bi} & \mathbf{1} & \mathbf{0} \\ \boldsymbol{\ell}_p^{\times}\mathbf{C}_{pi} & \mathbf{0} & \mathbf{1} \end{bmatrix}}_{\boldsymbol{\Delta}} \qquad (16) \\
&= \tilde{\mathbf{S}}^{\mathsf{T}}\boldsymbol{\Delta}. \qquad (17)
\end{aligned}$$

Substituting Eqs. (4) and (17) into Eq. (15), and premultiplying by $\tilde{\mathbf{S}}^{-\mathsf{T}}$ (where we assume that $\tilde{\mathbf{S}}$ is invertible) gives

$$\boldsymbol{\Delta}(\mathbf{M}\boldsymbol{\Pi}\dot{\tilde{\boldsymbol{\nu}}}+\mathbf{M}\dot{\boldsymbol{\Pi}}\tilde{\boldsymbol{\nu}}+\boldsymbol{\Omega}\mathbf{M}\boldsymbol{\Pi}\tilde{\boldsymbol{\nu}}+\mathbf{a})=\boldsymbol{\Delta}(\bar{\boldsymbol{\tau}}_b^d+\bar{\boldsymbol{\tau}}_b^c), \tag{18}$$

where

$$\dot{\boldsymbol{\Pi}}=\begin{bmatrix}\mathbf{C}_{bi}^{\mathsf{T}}\boldsymbol{\omega}_b^{bi^\times}\mathbf{y}_b^\times & -\mathbf{C}_{pi}^{\mathsf{T}}\boldsymbol{\omega}_p^{pi^\times}\boldsymbol{\ell}_p^\times\\ \mathbf{0} & \mathbf{0}\\ \mathbf{0} & \mathbf{0}\end{bmatrix}.$$

We let $\tilde{\mathbf{M}}(\boldsymbol{\theta}^{bi},\boldsymbol{\theta}^{pi})=\boldsymbol{\Delta}\mathbf{M}\boldsymbol{\Pi}$, $\tilde{\boldsymbol{\tau}}_{non}=\boldsymbol{\Delta}\left(\mathbf{M}\dot{\boldsymbol{\Pi}}\tilde{\boldsymbol{\nu}}+\boldsymbol{\Omega}\mathbf{M}\boldsymbol{\Pi}\tilde{\boldsymbol{\nu}}+\mathbf{a}\right)$, $\tilde{\boldsymbol{\tau}}_b^d=\boldsymbol{\Delta}\bar{\boldsymbol{\tau}}_b^d$ and $\tilde{\boldsymbol{\tau}}_b^c=\boldsymbol{\Delta}\bar{\boldsymbol{\tau}}_b^c$, then the equations of motion in terms of the independent generalized coordinates can be written as

$$\tilde{\mathbf{M}}(\boldsymbol{\theta}^{bi},\boldsymbol{\theta}^{pi})\dot{\tilde{\boldsymbol{\nu}}}+\tilde{\boldsymbol{\tau}}_{non}=\tilde{\boldsymbol{\tau}}_b^d+\tilde{\boldsymbol{\tau}}_b^c. \tag{19}$$

To validate these equations a simulation was conducted with zero disturbances and non-zero initial conditions to verify that the energy of the system remained constant.

4. ESTIMATION

Recall from Eq. (2), the kinematics of $\mathscr{R}$ obey [2]

$$\dot{\mathbf{C}}_{bi}=-\boldsymbol{\omega}_b^{bi^\times}\mathbf{C}_{bi}.$$

For the sake of simplicity in notation, we will neglect the subscripts and superscripts such that the kinematics can be rewritten as

$$\dot{\mathbf{C}}=-\boldsymbol{\omega}^\times\mathbf{C}.$$

Let $\underrightarrow{g}$ and $\underrightarrow{m}$ be the direction unit physical vectors corresponding to the Earth's gravitational acceleration and magnetic field respectively. We measure $\underrightarrow{g}$ and $\underrightarrow{m}$ in the body frame. Therefore we have,

$$\mathbf{g}_b^y=\mathbf{C}\mathbf{g}_i+\boldsymbol{\mu}^g\quad\text{and}\quad\mathbf{m}_b^y=\mathbf{C}\mathbf{m}_i+\boldsymbol{\mu}^m,$$

where $\mathbf{g}_b^y\in\mathbb{R}^3$ and $\mathbf{m}_b^y\in\mathbb{R}^3$ are normalized and correspond to the measurements expressed in the body frame, and $\boldsymbol{\mu}^g\in\mathbb{R}^3$ and $\boldsymbol{\mu}^m\in\mathbb{R}^3$ are zero mean Gaussian noise associated with the measurements. We assume $\boldsymbol{\mu}^g\sim\mathscr{N}(\mathbf{0},\mathbf{R}^g)$ and $\boldsymbol{\mu}^m\sim\mathscr{N}(\mathbf{0},\mathbf{R}^m)$. We also measure angular velocity,

$$\boldsymbol{\omega}^y=\boldsymbol{\omega}+\boldsymbol{\mu}^\omega,$$

where $\boldsymbol{\omega}^y=[\omega_1^y\ \ \omega_2^y\ \ \omega_3^y]^{\mathsf{T}}$ is the measured angular velocity and $\boldsymbol{\mu}^\omega\sim\mathscr{N}(\mathbf{0},\mathbf{R}^\omega)$ is the noise associated with the gyroscope measurement. We will now implement the estimator dynamics proposed in [7]. The estimator proposed in [7] includes gyroscope bias compensation, however, we have not included this in our formulation. The gyroscope bias will be considered in the future. Let

$$\dot{\hat{\mathbf{C}}}=-(\boldsymbol{\omega}^y+\boldsymbol{\sigma})^\times\hat{\mathbf{C}}=-\hat{\boldsymbol{\omega}}^\times\hat{\mathbf{C}},$$

where $\hat{\boldsymbol{\omega}}=\boldsymbol{\omega}^y+\boldsymbol{\sigma}$, $\hat{\mathbf{C}}$ is the estimate of $\mathbf{C}$, and $\boldsymbol{\sigma}$ is the innovation. The goal is to drive $\hat{\mathbf{C}}$ to $\mathbf{C}$. We will choose $\boldsymbol{\sigma}$ as [7, 9]

$$\boldsymbol{\sigma}=-k\left(k_g\hat{\mathbf{g}}_b^\times\mathbf{g}_b^y+k_m\hat{\mathbf{m}}_b^\times\mathbf{m}_b^y\right),$$

where

$$\hat{\mathbf{g}}_b=\hat{\mathbf{C}}\mathbf{g}_i\quad\text{and}\quad\hat{\mathbf{m}}_b=\hat{\mathbf{C}}\mathbf{m}_i,$$

Table 1. Physical properties of the platform model.

Property	Value	Units
$\boldsymbol{\ell}_p$	$[0\ \ 2\ \ 0]^{\mathsf{T}}$	m
$\mathbf{y}_b$	$[0\ \ 0\ \ 0.0577]^{\mathsf{T}}$	m
$m_{\mathscr{R}}$	6	kg
$\mathbf{I}_b^{\mathscr{R}b}$	$\mathrm{diag}\{0.0161, 0.0163, 0.0112\}$	kg·m^2
$m_{\mathscr{P}}$	0.1	kg
$\mathbf{J}_p^{\mathscr{P}p}$	$\mathrm{diag}\{0.133,\ 5\times10^{-6},\ 0.133\}$	kg·m^2

are the estimates of $\mathbf{g}_i$ and $\mathbf{m}_i$ expressed in the body frame, and $0 < k < \infty$, $0 < k_g < \infty$ and $0 < k_m < \infty$ are constants.

In practice, the estimation will be done in discrete time, therefore it is necessary to discretize the estimator dynamics. Let T denote the sample time and assume that $\hat{\boldsymbol{\omega}} = \hat{\boldsymbol{\omega}}^k$ for $t \in [kT, (k+1)T]$ then the discrete time estimator dynamics are given by [7, 9],

$$\hat{\mathbf{C}}^{k+1} = \mathbf{A}^k \hat{\mathbf{C}}^k,$$

where $\mathbf{A}^k = \exp(\hat{\boldsymbol{\omega}}^{k^\times})$ is given by [11]

$$\mathbf{A}^k = \mathbf{1} - \hat{\boldsymbol{\omega}}^{k^\times} \frac{\sin(|\hat{\boldsymbol{\omega}}^k|T)}{|\hat{\boldsymbol{\omega}}^k|} + \left(\hat{\boldsymbol{\omega}}^{k^\times}\right)^2 \frac{1-\cos(|\hat{\boldsymbol{\omega}}^k|T)}{|\hat{\boldsymbol{\omega}}^k|^2}.$$

5. CONTROL

The atmospheric balloon platform is equipped with a single brushless DC motor which will be used as a reaction wheel to control the yaw angle of the platform. Therefore, let $\boldsymbol{\tau}_b^c = [0\ \ 0\ \ \tau_c]^{\mathsf{T}}$. Now, consider the following PD type control law:

$$\tau_c = -k_p \hat{\theta}_3 - k_d \omega_3^y,$$

where $\hat{\theta}_3$ is the estimated yaw angle of the platform extracted from $\hat{\mathbf{C}}$, ω_3^y is the third component of the measured angular velocity, and k_p and k_d are constants such that $0 < k_p < \infty$ and $0 < k_d < \infty$.

6. SIMULATION RESULTS

The estimation algorithm and control law previously presented will now be implemented in a simulation of the balloon platform. The physical properties of the platform and pendulum system are shown in Table 1. The initial angular velocity is $\boldsymbol{\omega}_b(0) = [0\ \ 0\ \ 0.1]^{\mathsf{T}}$ rad/s and the initial attitude is $\mathbf{C}_{bi,0} = \mathbf{C}_1(0^\circ)\mathbf{C}_2(0^\circ)\mathbf{C}_3(20^\circ)$, where $\mathbf{C}_i,\ i = 1,\ 2,\ 3$ are principal rotations about the 1, 2 and 3 axes. The desired attitude of the platform is $\mathbf{C}_{di} = \mathbf{C}_1(\theta_1)\mathbf{C}_2(\theta_2)\mathbf{C}_3(0^\circ)$ where θ_1 and θ_2 are arbitrary. The initial pendulum attitude is $\mathbf{C}_{pi,0} = \mathbf{C}_1(-88^\circ)\mathbf{C}_2(0^\circ)\mathbf{C}_3(0^\circ)$ and its initial angular velocity is $\boldsymbol{\omega}_p(0) = [0\ \ 0\ \ 0]^{\mathsf{T}}$. During simulation, this plant model is numerically integrated using a fourth-order Runge–Kutta integrator with a time-step of 0.005 s.

For the observer, we set $k = 10$, $k_g = 1$ and $k_m = 0.5$. The initial estimate of the attitude is $\hat{\mathbf{C}}_0 = \mathbf{1}$. The measurement noise covariance matrices associated with the accelerometer, magnetometer and gyroscope are $\mathbf{R}^g = \mathrm{diag}\{\sigma_g^2,\ \sigma_g^2,\ \sigma_g^2\}$, $\mathbf{R}^m = \mathrm{diag}\{\sigma_m^2,\ \sigma_m^2,\ \sigma_m^2\}$ and $\mathbf{R}^\omega = \mathrm{diag}\{\sigma_\omega^2,\ \sigma_\omega^2,\ \sigma_\omega^2\}$ respectively, where $\sigma_g = \sigma_\omega = 0.005$ and $\sigma_m = 0.01$. We will assume that $\mathbf{g}_i = [0\ \ 0\ \ -1]^{\mathsf{T}}$ and $\mathbf{m}_i = 1/\sqrt{3}[1\ \ 1\ \ 1]^{\mathsf{T}}$ for all time. The control gains are set to $k_p = 1.5$ and $k_d = 0.5$. We will consider the estimation and control algorithms to be running on an onboard computer at a frequency of 25 Hz. Therefore, during the simulation

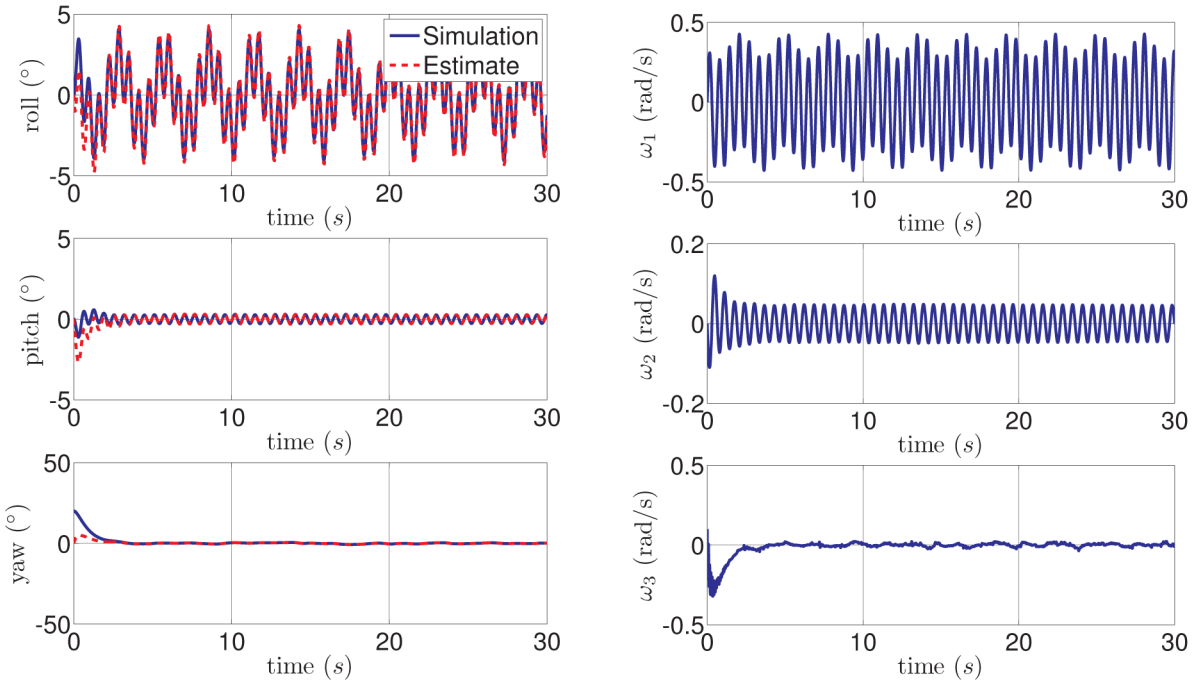

(a) (b)

Fig. 2. (a) Euler angles and (b) angular velocity versus time.

the measurements are acquired and the control commands are updated every 0.04 s.

The disturbances are assumed to be of the form $\boldsymbol{\tau}_b^d = [0 \;\; 0 \;\; \tau_d]^\mathsf{T}$ which is based on data taken during an uncontrolled preliminary flight. Details of this flight can be found in [12]. Nominally, the platform dynamics obey

$$I_3 \dot{\omega}_3^y = \tau_d, \tag{20}$$

where $I_3 = 0.0122$ kg·m^2. The measured angular acceleration, $\dot{\omega}_3^y$, can be approximated at any time, t^k, in terms of the gyroscope measurements as

$$\begin{aligned} \dot{\omega}_3^{y,k} &\approx \frac{\omega_3^{y,k} - \omega_3^{y,k-1}}{t^k - t^{k-1}} \\ &= \frac{\omega_3^{y,k} - \omega_3^{y,k-1}}{\Delta T}, \end{aligned}$$

where $\Delta T = 0.04$ s is the sampling time. Now, τ_d can be approximated from Eq. (20) by

$$\tau_d^{k+1} = I_3 \frac{\omega_3^{y,k+1} - \omega_3^{y,k}}{\Delta T}.$$

The disturbance torques are populated using angular velocity measurements taken at an altitude of about 20 km over a period of 30 s. This data set is pretreated to remove outlying data points and the disturbance torque at any time is found by interpolation during simulation.

The Euler angles as well as their estimates are shown in Fig. 2(a). Note that the estimates converge to their true counterparts and that the yaw angle of the platform approaches 0°, its desired value. The angular

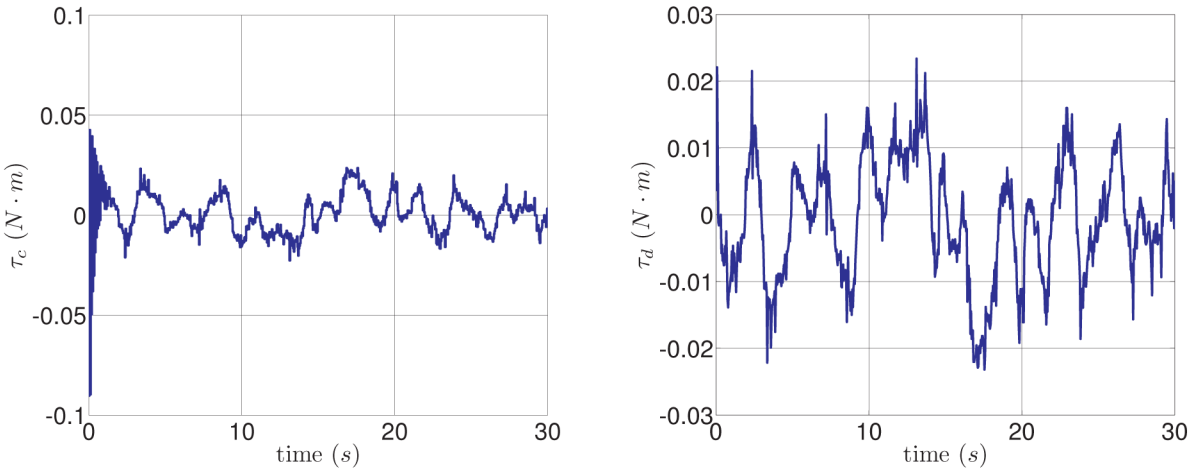

Fig. 3. (a) Control and (b) disturbance torques versus time.

velocity of the balloon platform is shown in Fig. 2(b). Since no viscous drag has been modelled there is no damping in the pitch and roll angles and they continue to oscillate. Although the yaw angle of the platform approaches zero, its angular velocity is not exactly zero due to the high disturbance torques. The control and disturbance torques are shown in Fig. 3. It should be noted that these results are theoretical, and represent a preliminary investigation into the dynamics, estimation and control of the real McHAB balloon platform. Actual test flight data could be used to verify the accuracy of these simulations. This is a low fidelity model as many effects remain unmodelled, including the dynamics of the balloon itself. In the future, the model will be expanded upon to include balloon dynamics and will be used to construct more advanced control techniques as well as to validate their performances.

7. CONCLUSIONS

In this paper the dynamic modelling, estimation, and control of an atmospheric balloon platform has been investigated. Accelerometer, magnetometer and gyroscope measurements were used to construct the estimator proposed in [7, 9], and a simple PD control law was implemented to control the yaw angle of the platform. As mentioned in Section 1, the contribution of this work is the implementation of the estimator in combination with yaw control on an atmospheric balloon platform system. It was shown, through numerical simulation, that the estimator converged to the true state values and the yaw angle of the platform was successfully controlled. In the future, this model may serve as a base for the application of more advanced control techniques.

ACKNOWLEDGEMENTS

The authors would like to thank the reviewers for their comments which have greatly improved this paper, as well as François Hogan for translating the abstract.

REFERENCES

1. Wertz, J.R., *Spacecraft Attitude Determination and Control*, D. Reidel Publishing Company, Dordrecht, The Netherlands, 1978.
2. Hughes, P.C., *Spacecraft Attitude Dynamics* (2nd ed.). Dover, Mineola, New York, 2004.

3. Crassidis, J.L. and Junkins, J.L., *Optimal Estimation of Dynamic Systems* (2nd ed.). CRC Press, Taylor and Francis Group, Boca Raton, FL, 2012.
4. Quine, B.M., Strong, K., Wiacek, A., Wunch, D., Anstey, J.A. and Drummond, J.R., "Scanning the Earth's limb from a high-altitude balloon: The development and flight of a new balloon-based pointing system", *Journal of Atmospheric and Oceanic Technology*, Vol. 19, No. 5, pp. 618–632, 2002.
5. Pascale, E., Ade, P., Bock, J., Chapin, E., Chung, J., Devlin, M., Dicker, S., Griffin, M., Gundersen, J., Halpern, M. et al., "The balloon-borne large aperture submillimeter telescope: BLAST", *The Astrophysical Journal*, Vol. 681, No. 1, p. 400, 2008.
6. Buccilli, T., Folina, A., Medaglia, E., Montefusco, P., Oliva, M., Palmerini, G. and Sestito, A., "A low cost inertial navigation experiment onboard balloons", in *Proceedings of the 19th ESA Symposium on European Rocket and Balloon Programmes and Related Research*, Bad Reichenhall, Germany, 2009.
7. Mahony, R., Hamel, T. and Pflimlin, J.M., "Complementary filter design on the special orthogonal group SO(3)", in *Proceedings of the IEEE Conference on Decision and Control, and the European Control Conference*, Seville, Spain, December 12–15, pp. 1477–1484, MoC03.3, 2005.
8. Khosravian, A. and Namvar, M., "Globally exponential estimation of satellite attitude using a single vector measurement and gyro", in *Proceedings of the IEEE Conference on Decision and Control*, Atlanta, GA, December 15–17, pp. 364–369, 2010.
9. Hamel, T. and Mahony, R., "Attitude estimation on SO(3) based on direct inertial measurements", in *Proceedings of the IEEE International Conference on Robotics and Automation*, Orlando, FL, May 15–19, pp. 2170–2175, 2006.
10. Mahony, R., Hamel, T. and Pflimlin, J.M., "Nonlinear complementary filters on the special orthogonal group", *IEEE Transactions on Automatic Control*, Vol. 53, No. 5, pp. 1203–1218, June 2008.
11. Murray, R., Li, Z. and Sastry, S., *A Mathematical Introduction to Robotic Manipulation*, CRC, 1994.
12. Tran, N.K., He, X., Zlotnik, D.E. and Forbes, J.R., "Attitude sensing and control of a stratospheric ballon platform", in *Proceedings AIAA Balloon Systems Conference*, Daytona Beach, FL, March 26–28, 2013.
13. Forbes, J., Barfoot, T. and Damaren, C., "Dynamic modeling and stability analysis of a power-generating tumbleweed rover", *Multibody System Dynamics*, Vol. 24, pp. 413–439, 2010.
14. Chaturvedi, N., Lee, T., Leok, M. and McClamroch, N., "Nonlinear dynamics of the 3D pendulum", *Journal of Nonlinear Science*, Vol. 21, No. 1, pp. 3–32, 2011.
15. De Jalon, J.G. and Bayo, E., *Kinematic and Dynamic Simulation of Multibody Systems*, Springer-Verlag, 1994.
16. Angeles, J. and Lee, S., "The modelling of holonomic mechanical systems using a natural orthogonal complement", *Transactions of the Canadian Society for Mechanical Engineering*, Vol. 13, No. 4, pp. 81–89, 1989.